

Article

# Surface Characterization and Bulk Property Analysis of Aluminum Powders Treated with Hydrophobic Coatings: Stearic Acid and Phenyl-Phosphonic Acid

Bellamarie Ludwig 

The Applied Research Laboratory, The Pennsylvania State University, State College, PA 16804, USA; bxb234@psu.edu; Tel.: +1-814-865-7299

**Abstract:** Stearic and phenyl-phosphonic acids were applied to fine aluminum particles to understand their effect on the surface chemical composition and bulk properties of the surface-treated powders. During the solution phase deposition process, the surface composition changes chemically through a condensation reaction between the acid and particle surface hydroxyl groups, forming covalent chemical bonds. The retention of both types of acids was verified through characterization using Fourier transform infrared spectroscopy (FTIR) and X-ray photoelectron spectroscopy (XPS). The presence of stearic acid on the particle surface was observed through signature absorbance peaks, including interfacial C-O bonding modes, carboxylate, and carbonyl moieties, all present on both the treated powder. Spectra using XPS showed an increase in -CH relative intensity signal on the particle surface when compared to the raw material when considering the carbon 2p photoelectron peak. Similar findings confirmed the presence of the phenyl-phosphonic acid when comparing to the raw material. The IR spectrum confirmed the presence of P-O-Al, P-O, and phosphonates as a result of the surface bonding between the reagent and particles. XPS always provided evidence through the presence of phosphorous 2p and 2s photoelectron peaks at 191.3 and 133.4 eV, respectively. The bulk properties of both surface treated powders improved, as shown through improved apparent/tap density and a decreased Hausner Ratio (Group C to Group A behavior). Rheological characterization provided additional evidence by showing a reduced specific energy, flow rate index, and cohesion. The particle packing was improved as evidenced through reduced compressibility as a function of applied normal stress.



check for updates

**Citation:** Ludwig, B. Surface Characterization and Bulk Property Analysis of Aluminum Powders Treated with Hydrophobic Coatings: Stearic Acid and Phenyl-Phosphonic Acid. *Solids* **2024**, *5*, 1–13. <https://doi.org/10.3390/solids5010001>

Academic Editor: Joaquim Carneiro

Received: 6 November 2023

Revised: 15 December 2023

Accepted: 19 December 2023

Published: 22 December 2023



**Copyright:** © 2023 by the author. Licensee MDPI, Basel, Switzerland. This article is an open access article distributed under the terms and conditions of the Creative Commons Attribution (CC BY) license (<https://creativecommons.org/licenses/by/4.0/>).

**Keywords:** molecular spectroscopy; aluminum; surface coatings; stearic acid; phenyl-phosphonic acid

## 1. Introduction

The use of coatings to alter the physical or chemical properties of surfaces is a common practice [1–4]. Specifically, fine particle-sized powdered materials can have surface characteristics that impede their use in a wide variety of flow, delivery, and filling applications. Altering the surface properties with submicron-sized coatings can change the interfacial behavior between particles while maintaining the core material for the intended use. In many cases, phenomena such as capillary bridging, water adsorption, and intrinsic hydrophilicity can be mitigated by the deposition of hydrophobic coatings. As a result of hydrophobic treatment, surface treated powders tend to show improved flow behavior. In this work, the use of two common surface coating agents was considered based on carboxylic and phosphonic acids groups to coat aluminum powders for improved flow behavior.

Aluminum powder has uses in several critical industries, including pyrotechnics, additive manufacturing, and paint pigments. As the particle size decreases, the aluminum oxide passivation layer becomes susceptible to interparticulate forces more so than larger particles; the increased surface area of fine particles leads to increased contributions from electrostatic, Van der Waals, and surface chemical interactions. Previous work has shown

that siloxane based reagents can improve the flow properties of aluminum powder [5–8]. The silanes and siloxane reagents used in the aforementioned work contain aliphatic groups; thus, the use of other reagents containing similar groups are also of interest.

For large-scale processing, inexpensive and chemically benign surface treatment reagents are ideal. To that end, stearic acid (SA) was selected as potential candidate for improving the flow properties of aluminum powder. SA contains an aliphatic tail, with has been shown to produce hydrophobic surfaces needed to enhance flow behavior and reduce cohesion. The interaction of SA with alumina and aluminum powder oxide surfaces has been investigated previously [9–11]. Carboxylic acids interact with aluminum oxide surfaces and form an interfacial carboxylate through surface hydroxyl groups [12–14].

Similarly to SA, phosphonic acids interact with aluminum oxide surfaces through the acidic head group with surface hydroxyl groups on the oxide [15–18]. Due to the three oxygen atoms available to form the bonds between the surface and pendant groups, phosphonic acids are also more acidic than carboxylic acids and form hydrolytically stable bonds. Phenyl-phosphonic acid (PPA) is a common coating for corrosion protection and surface modification, including hydrophobicity [19].

This investigation focuses on the properties of surface treated aluminum powders through the use of surface characterization and powder rheology. Beyond the interest in different surface chemistry, these coatings can also provide other ideal properties, such as improved shelf life due to reduced aging from the coatings protective properties.

## 2. Materials and Methods

### 2.1. Materials

Ethanol (99.5%, <0.1% water, KOPTEC, Decon Labs., King of Prussia, PA, USA), stearic acid (98%, Alfa-Aesar, Haverhill, MA, USA), phenyl-phosphonic acid (98%, Sigma Aldrich, St. Louis, MO, USA), and aluminum powder (99.7%,  $d_{50} = 20 \mu\text{m}$ , 99% -325, Valimet, Stockton, CA, USA) were all used as received. All glassware was rinsed with ethanol and dried at 100 °C for 24 h prior to use. Hirsch funnels were rinsed thoroughly with the appropriate solvent prior to filtering the aluminum–slurry solutions.

### 2.2. Stearic Acid (SA-Al)

The stearic acid (SA,  $\text{C}_{17}\text{H}_{35}\text{COOH}$ ) solution (1 wt.%) was prepared by dissolving the SA powder in ethanol and stirring for 1 h in a warm water bath to completely dissolve the solute. Aluminum powder (50 g) was immersed in the solution at room temperature (25 °C) at a density of 1.0 g/10 mL and stirred in a round bottom flask for 2 h. The resulting solution was filtered using a standard Hirsch funnel and the product was rinsed thoroughly with ethanol to remove any physically absorbed SA. The powder was dried overnight at 100 °C in a standard oven and sieved prior to chemical and bulk property analysis.

### 2.3. Phenyl-Phosphonic Acid (PPA-Al)

The phenyl-phosphonic acid (PPA,  $\text{C}_6\text{H}_7\text{O}_3\text{P}$ ) solution (1 wt.%) was prepared in the same manner as the SA deposition solution. The powder (50 g) was dispersed in the solution for 24 h at room temperature (25 °C) at density of 1.0 g/10 mL as described by Thissen [20]. Using a Hirsch funnel, the resulting solution was filtered and rinsed with ethanol to remove physically absorbed PPA. After drying overnight at 100 °C, the powder was sieved prior to chemical and bulk property analysis.

### 2.4. Diffuse Reflectance Infrared Spectroscopy

Diffuse reflectance infrared spectroscopy (DRIFTS) measurements were collected using a Fourier transform infrared spectrophotometer (Bruker, Vertex V70, Billerica, MA, USA) equipped with a mercury-cadmium-telluride (MCT) detector. All spectra were collected in a Praying Mantis (Harrick Scientific, Pleasantville, NY, USA) accessory equipped with a closed environment sample chamber, which could be purged continuously with argon. The sample chamber windows were composed of  $\text{CaF}_2$ , which has a  $900 \text{ cm}^{-1}$  cutoff. The

spectrum resolution was set to  $6\text{ cm}^{-1}$  and 400 scans were performed. Powdered potassium bromide (KBr) was used for reference spectra and dried to  $350\text{ }^{\circ}\text{C}$  for 30 min prior to use. Additional KBr spectra were collected to enable in situ subtraction of atmospheric water contributions.

### 2.5. X-ray Photoelectron Spectroscopy

X-ray photoelectron spectroscopy (XPS) was performed using a Kratos Axis Ultra (Kratos Analytical Ltd., Stretford, UK) instrument with a monochromatic Al  $K_{\alpha}$  X-ray source and powdered samples were mounted on a silicon substrate using double sided tape (3M). Analysis was performed at a constant system pressure of  $10^{-8}$  torr and the pass energy for the survey scans were at 80 eV and with a step size of 0.5 eV; high resolutions scans were collected 20 eV and with a step size of 0.1 eV for high resolution. Charge correction was employed using the C 1s peak as an internal standard at 284.8 eV.

### 2.6. Bulk Density

The apparent ( $\rho_A$ ) and tap ( $\rho_T$ ) density measurements were completed using an Autotap<sup>TM</sup> (Quantachrome, Boynton Beach, FL, USA); Powder samples of 100 g of each sample were loaded into a 100 mL graduate cylinder and the apparent density reported. The sample was tapped until there was no longer an observable change in the density, which occurred beyond 3000 taps based on the ASTM–2006 standard [21]. The Hausner Ratio ( $H_R$ ) was calculated based on the following equation [22]:

$$H_R = \rho_T / \rho_A \quad (1)$$

where:

$H_R$  = Hausner Ratio (unitless)

$\rho_T$  = Tap density (g/cc)

$\rho_A$  = Apparent density (g/cc)

The calculated Hausner ratio results in the following classification (Table 1).

**Table 1.** Hausner Ratio designations based on the apparent and tap density.

Value	Group	Designation
>1.4	C	Cohesive
1.4–1.25	A–C	Transition Group
<1.25	A	Aeratable

### 2.7. FT4 Powder Rheometer<sup>®</sup> Measurements

The FT4 Powder Rheometer<sup>®</sup> (Tewkesbury, UK) was used to assess the raw and surface treated powder properties for density, flowability, and compressibility. The rheometer consists of a cylindrical sample holder, conditioning/measurement blade, and calibrated sensors to measure the torque and force against the blade whilst it transverses the powder column. Using the stability and variable flow rate test, the conditioned bulk density, specific energy, flow rate index, and stability index were determined. The conditioned bulk density is measured similarly to a typical bulk density; however, the powder has been conditioned by the FT4 blade to remove any loading irregularities. The standard FT4 stability and variable rate tests developed by Freeman Technologies were used as designed. The powder samples (100–150 g) were loaded into the rheometer's glass powder sample holder (50 mm diameter, borosilicate) and split using the sample holder splitter to ensure a level surface and the program run as designed using seven test cycles. The torque and force are measured as the blade travels through the powder, which can subsequently be integrated over the column height, resulting in an energy value.

The specific energy value evaluates the unrestricted powder properties as the measurement is taken during the upward cycle of the blade traverse. The value is represented

by an energy value as a function of mass (mJ/g). In general, a high specific energy signifies that the powder is more cohesive than free flowing.

The stability and flow rate indices can also be extracted from the test data; the stability index (SI) can be found in Equation (2). The SI measures quantitatively how the powder changes over multiple conditioning cycles. Typical changes include attrition, degradation, or forced agglomeration due to constant the agitation from the blade. When the changes are small, the index value will be approximately 1.0. In general, a stability index from 0.9 to 1.1 is considered a stable powder. Anything greater than 1.1 or less than 0.9 represents a powder that is considered unstable and may change during typical handling operations.

$$SI = BFE_7 / BFE_1 \quad (2)$$

where:

SI = Index (-)

$BFE_7$  = BFE after seven cycles (mJ)

$BFE_1$  = BFE after one cycle (mJ)

The flow rate index (FRI) measures changes in energy based on the tip speed whilst traversing the powder column. The flow energy is measured at four different tip speeds, including 10, 40, 70, and 100 mm/s. The ratio of the high and low tip speeds represents the FRI (Equation (3)). If the flow increases changes as the tip speed decreases, then the powder is likely cohesive ( $SI > 3$ ). When the difference between the high and low tip speeds is small, then the powder has less cohesive properties (approximately 1.5–3.0).

$$FRI = FE_{10\text{mm/s}} / FE_{100\text{mm/s}} \quad (3)$$

where:

FRI = Index (-)

$FE_{10}$  = FE after 10 mm/s tip speed (mJ)

$FE_{100}$  = FE after 100 mm/s tip speed (mJ)

In order to measure shear properties, the typical blade is replaced with a rotational shear head with multiple blades to measure plastic deformation as a function of applied normal stress. As the powder bed fails, the shear stress is measured similarly to the BFE and FE. The incipient shear stress is measured at five different applied normal stresses to generate a linear fit equation. From this, the cohesion, or the shear stress value at zero applied normal stress, can be calculated. In addition, Mohr–Coulomb circle analysis can be used to extrapolate other properties such as the flow factor. The samples (100–150 g) were loaded into the 50 mm shear measurement sample holder and split similarly to the variable flow rate and stability tests.

To measure compressibility, a vented piston is used instead of the blade to allow air release from the powder as it is compressed by applied normal stress. With changes in powder column height as a result of applied normal stress, the powder density changes and is reported as percentage change. For this particular set of samples, the applied normal stress was measured from 0.5 to 8.0 kPa.

All measurements completed on the samples used in this work were repeated at least three times. Error bars are reported in the figures where appropriate and represent the standard deviation.

### 3. Results and Discussion

#### 3.1. Surface Characterization

To verify the presence of the surface treatment agent on the particle surfaces DRIFTS was used to investigate the surface chemical properties. Figure 1a reveals the DRIFTS spectra for SA-Al powder and neat SA in the 1800–1300  $\text{cm}^{-1}$  region where the carboxylic acid and carboxylate vibrational modes were anticipated. Table 2 contains the vibrational assignments for the carboxyl and carboxylate absorbance peaks or bands results. The following important absorbance peaks were observed: (1) 1700  $\text{cm}^{-1}$  for  $\nu_{C=O}$  (2) 1470  $\text{cm}^{-1}$  for  $\nu_{C-O}$ , and (3) at 1430 and 1410  $\text{cm}^{-1}$  are attributed to  $\nu_{C-OH}$ , defor-

mation [23]. The SA treated powder contains multiple complex modes observed in the 1590–1510  $\text{cm}^{-1}$  region that are described pictorially in Figure 1b, 1–4. The presence of the large absorbance remaining at 1700  $\text{cm}^{-1}$  with a shoulder at 1688  $\text{cm}^{-1}$  suggests that physisorbed, non-interacting material is likely present on the surface. While the peak shape is sharper, it still has the same general shape with a maxima in close agreement with the neat powder. Multiple types of cleaning methods were attempted to remove the physisorbed material, including rinsing with various solvents and drying; however, only a partial decrease in intensity was observed. As reported previously in the literature [12] the peak at 1464  $\text{cm}^{-1}$  suggests a symmetric binding of the carboxylate with the oxide surface (Figure 1b, 3,4). There are five peaks located over a wider, broad absorbance in the 1590–1510  $\text{cm}^{-1}$  at 1584, 1562, 1545, 1525, and 1510  $\text{cm}^{-1}$ . Morterra et al. report that these peaks are permissibly close to both monodentate and bidentate types of  $\text{CO}_2$  on adsorbed on alpha and gamma alumina, suggesting similar type interactions observed on the SA treated powder [24]. These observations indicate that there are multiple types of interfacial bonding. It is likely that the orientation of the stearic acid is perpendicular to the particle surface, which can be corroborated by the carboxylate vibrational modes observed. This has been presented elsewhere with monolayer type coverages on planar surfaces [23]. However, a more detailed study of the surface is required to determine the orientation and conclusively determine binding modes, which is beyond the scope of this manuscript.

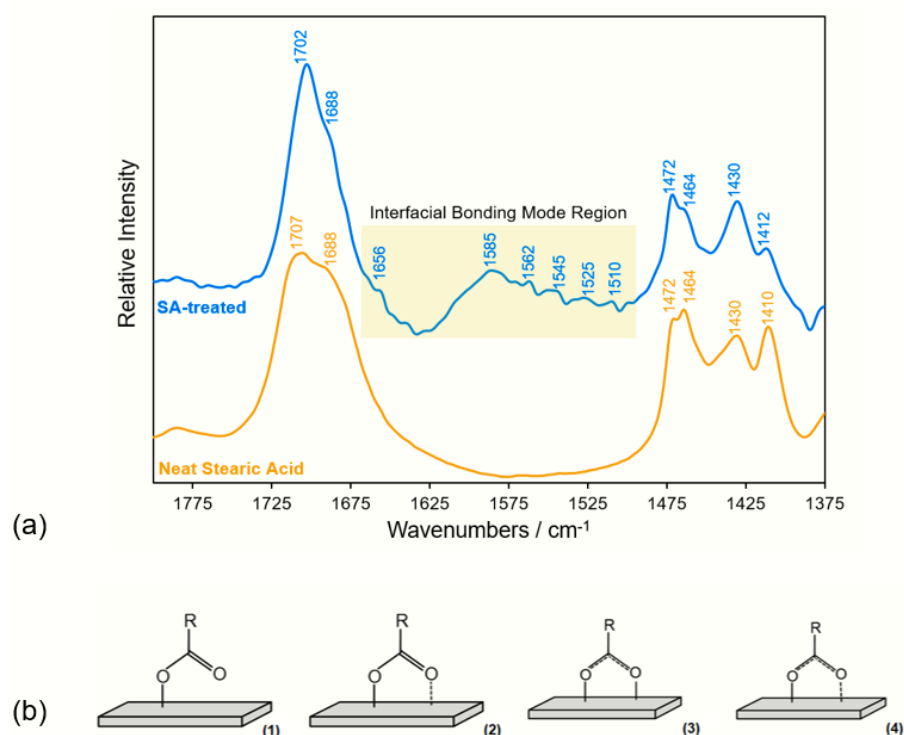


**Figure 1.** (a) DRIFTS spectra for SA–Al and reference spectrum of neat SA in the carboxylate region (1800–1300  $\text{cm}^{-1}$ ); (b) Various interfacial modes for interactions of carboxylic acids with aluminum oxide surface.

XPS analysis was used to further probe the surface structure and composition. The C 1s signal increased when compared to the raw powder, as seen in Figure 2. The raw powder contains an aliphatic, adventitious carbon peak at 284.8 eV, in addition to peaks at 286.8 and 289.0 eV for C–O and C=O type carbon, respectively. This is typically observed on raw aluminum powders and is attributed to atmospheric contamination and adventitious carbon. A large increase in the carbon content after SA surface treatment was observed and is due to the presence of the aliphatic tail present on SA. Figure 2 shows the high-resolution carbon 1s peak for the stearic acid treated aluminum powder (gold). The raw powder

has a lower aliphatic peak than the SA treated sample at 284.8 eV (blue). This indicates that the amount of aliphatic carbon on the sample increased, which is consistent with the presence of the alkyl chain component of SA. There is also a carbonyl peak at 289.0 eV, which can be attributed to the carboxylate head group associated with the particle surface. The C=O/C-C peak area ratio was calculated to infer additional information about the structure of the SA after deposition and drying. The ratio of C=O/C-C should be 0.055, based on the structure of the SA molecule, with 18 carbon atoms for every carboxylate group (1/18). The experimental data revealed a ratio of 0.059 (arb. units), which is close to the anticipated value.

**Table 2.** Absorbance peak and band assignments for C-O vibrational modes observed in the SA-Al sample spectrum; results show a mix of monodentate and bidentate bonding modes.

Label	Peak or Band ( $\text{cm}^{-1}$ )	References
$\nu_s(\text{COO}^-)$	1472	[12,13,23]
$\nu_a(\text{COO}^-)$	1510	[12,13,23]
$\nu_a(\text{COO}^-)$	1584	[12,13,23]
$\nu(\text{C}=\text{O})$	1656	[12,13,23]
$\nu(\text{C}=\text{O})$	1688	[12,13,23]
$\nu(\text{C}=\text{O})$	1702	[12,13,23]

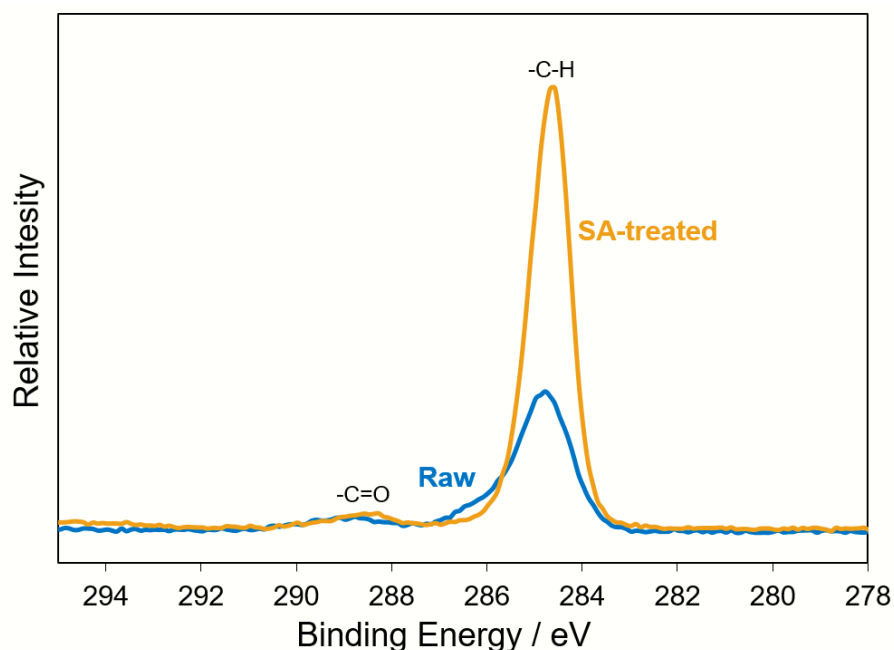


**Figure 2.** XPS high resolution spectra for SA-Al sample showing increased presence of -CH when compared to the raw powder sample.

Figure 3a shows the IR spectrum collected for the PPA-Al and Table 3 contains the vibrational assignments. The interfacial behavior of PPA and aluminum oxide in solution has been shown to produce phosphonate groups that are complexed at the surface, leaving the aromatic ring oriented vertically to the surface of the particle (Figure 3b) [15]. The IR spectrum contained an absorbance peak at  $\sim 1150 \text{ cm}^{-1}$  ( $\nu_{\text{P-O-Al}}$ ), which has been previously assigned at the vibration of the P-O-Al bond present on the surface of an alumina substrate [15]. The P-O absorbance from P-O-C<sub>6</sub>H<sub>6</sub> have been reported in the 994–855  $\text{cm}^{-1}$  wavenumber region, and likely accounts for the broad absorbance centered at  $\sim 940 \text{ cm}^{-1}$ , ( $\nu_{\text{s,P-O}}$ ) [25]. The absorbance values at 1258 ( $\nu_{\text{P=O}}$ ) and 1022 ( $\nu_{\text{a,P-O}}$ )  $\text{cm}^{-1}$  are likely from P-O stretches of the C-P(-O)<sub>3</sub> unit.

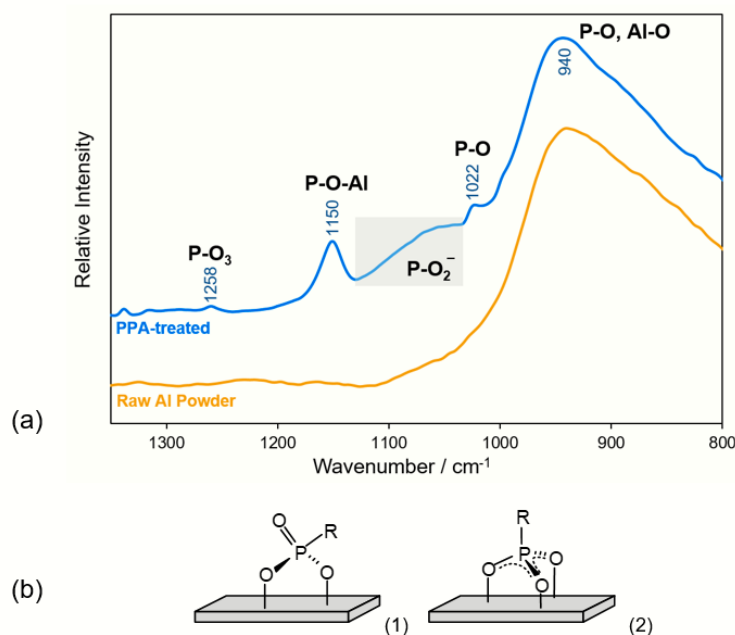


**Figure 3.** (a) DRIFTS spectrum of PPA–Al sample, showing absorbance peaks associated with P–O, PO<sub>2</sub><sup>−</sup> associated with the aluminum oxide surface. (b) Possible orientations and bonding modes of the phosphonate head group: (1) bidentate through P–O–Al and (2) complex through three oxygen atoms of the head group.

**Table 3.** Absorbance peak and band assignments for various P–O moieties observed in the PPA–Al sample spectrum.

Label	Peak or Band (cm <sup>−1</sup> )	References
$\nu_s(P-O)$	940	[19,26]
$\nu_a(P-O)$	1022	[19,26]
$\nu_{a,s}(P-O_2^-)$	1000–1070	[19,26]
$\nu(P-O-Al)$	1150	[15]
$\nu(P=O)$ , phosphonate	1258	[26]

XPS was used to verify the retention of P from PPA on the particle surfaces as shown in the survey and HR spectra in Figure 4a,b. Figure 4a reveals the survey spectrum in the P 2s and P 2p photoelectron region, with distinct peaks at B.E.s of 191.3 and 133.5 eV; R–Al did not have any detectable signal in these areas. Figure 4b shows the high resolution spectrum of the P 2p peak, where the B.E. for the peak observed was 133.8 eV, consistent with phosphonates and other literature references [27]. Using the C 1s peak to evaluate the presence of –CH, as shown in Figure 4b, the C/P ratio was calculated and results in a value of approximately 6.0 (arb. units). Based on the stoichiometry, this is close to the expected ratio for an aromatic ring attached to one P atom. Aromatic carbon with sp<sup>2</sup> hybridization is difficult to isolate from sp<sup>3</sup> carbon. The residual fit without deconvolution was 1.25, suggesting that a single peak was a good fit for the C 1s peak; however, additional characterization methods would be needed to unambiguously confirm that the absorbance peak can be assigned as sp<sup>2</sup> hybridized carbon. The low absorbance observed in the DRIFTS data made identification of aromatic –C–H difficult to resolve with complete certainty.

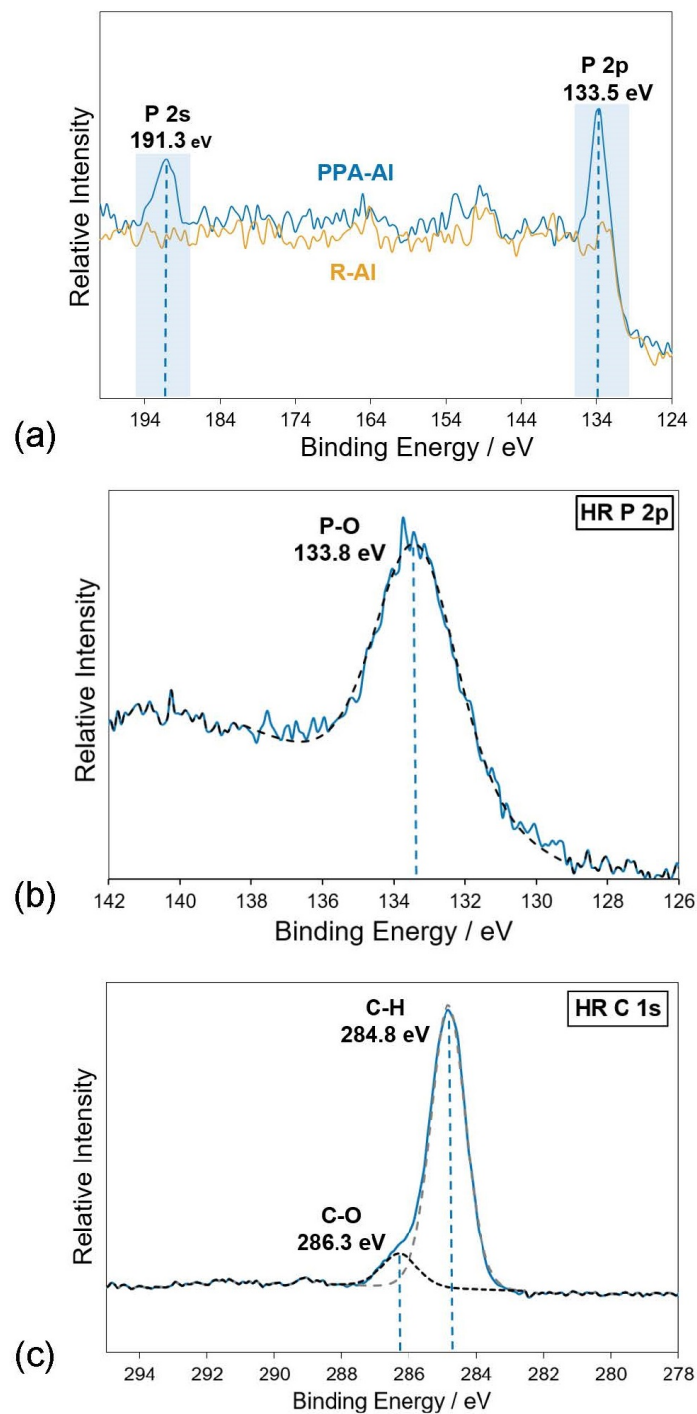


**Figure 4.** (a) Survey spectrum of PPA–Al powder, showing presence of 2s and 2p peaks for P at 191.3 and 133.5 eV; (b) high resolution P 2p photoelectron peak showing presence of P-O on the particle surface at a BE of 133.8; and (c) high resolution C 1s spectrum showing presence of -CH and -CO at 284.8 and 286.3 eV.

### 3.2. Comparison of Bulk Properties

Figure 5 shows the  $\rho_T$ ,  $\rho_a$ , and Hausner Ratio ( $H_R$ ) for each of the samples. The  $H_R$  values (Equation (1)) for the SA-Al and PPA-Al powders were reduced when compared to the raw material, resulting in group A designations. The values of  $\rho_a$  increased by 25% for SA-Al and 20% for PPA-Al; this increased in the apparent density value is due to the

improved particle packing and reduction in interstitial pores and voidage areas. Although not a direct measurement of flow, the  $H_R$  suggests that both materials ability to be fluidized was improved as a result of the surface treatment.

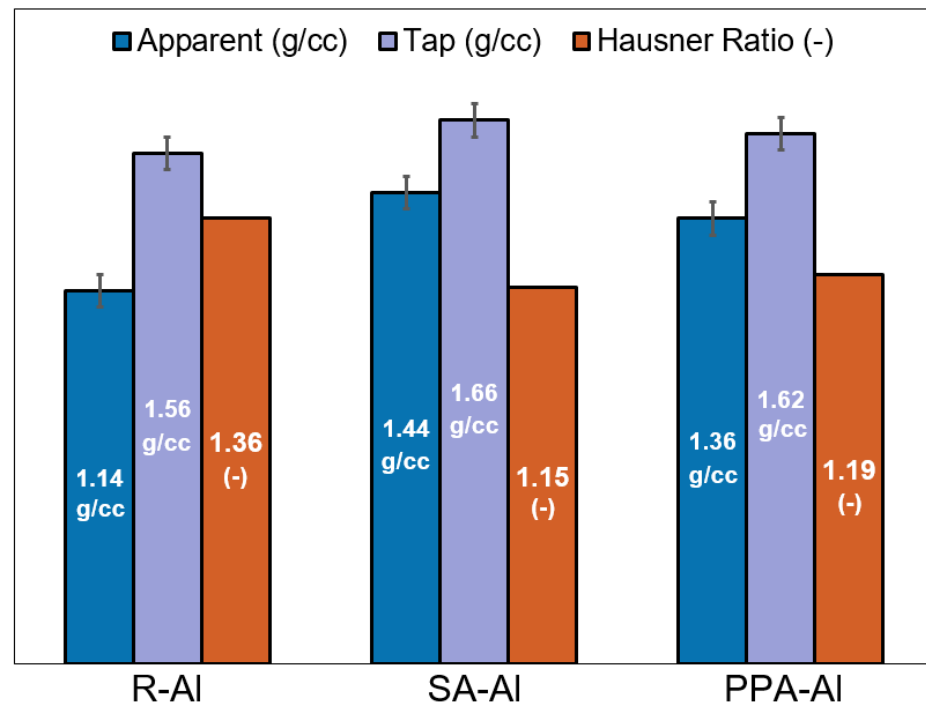


**Figure 5.** Comparison of density values for R–Al, SA–Al, and PPA–Al; Treated sample showed improved apparent density and Hausner ratio.

Characterization using powder rheology revealed additional insights into the flow changes resulting from surface treatment, as shown in Figure 6. When comparing the conditioned bulk density of the powders, there was a modest increase by 10% for SA-Al and 3% for PPA-Al. Comparing the apparent density as previously described, the values are much closer to the raw material; this is likely due to the preparation methods the FT4 utilizes. The rheometer conditions the powder through the descent/ascent through the powder column with a calibrated force sensor in the blade. This method is different from a poured density where the powder bed is disturbed during the loading process, allowing for release of air filled pockets and partial fluidization. The specific energy (SE) measures the resistance to the blade upon ascent through the powder column. This results in a total flowability energy value representing primarily interparticulate interactions rather than interactions with sample holder, which is then normalized to mass. By using the force calculated during the ascent, it represents a low stress environment and is more influenced by the powder's cohesivity than a packed state. When comparing the treated powders to the raw material, there was a decrease in SE by 28% for SA-Al and 25% for PPA-Al. Both SE values fall within experimental error of each other, suggesting a similar reduction in SE when compared to the reference material, as shown in Figure 6.

The stability and variable flow rate test produces indices based on the method structure and subsequent calculations. The test first cycles through seven identical conditioning cycles. The ratio of the initial flow energy to the final test energy is referred as the Stability Index (SI). If the flow energy is less than 0.9 or greater than 1.1, there are likely significant property changes to the material, including attrition, agglomeration, or caking. For all three materials, the SI remained within the range of a stable material at 0.95, 0.95, and 1.01 for R-Al, SA-Al, and PPA-Al, respectively, as shown in Figure 6.

The flow rate index (FRI) represents changes in the powder as a result of changing the blade speed as it moves through the powder column. The FRI was not significantly

influenced by the surface treatment as the values were close to the range of 1.5–3, which suggests a material that is not influenced by the changing blade speed (see Figure 6).

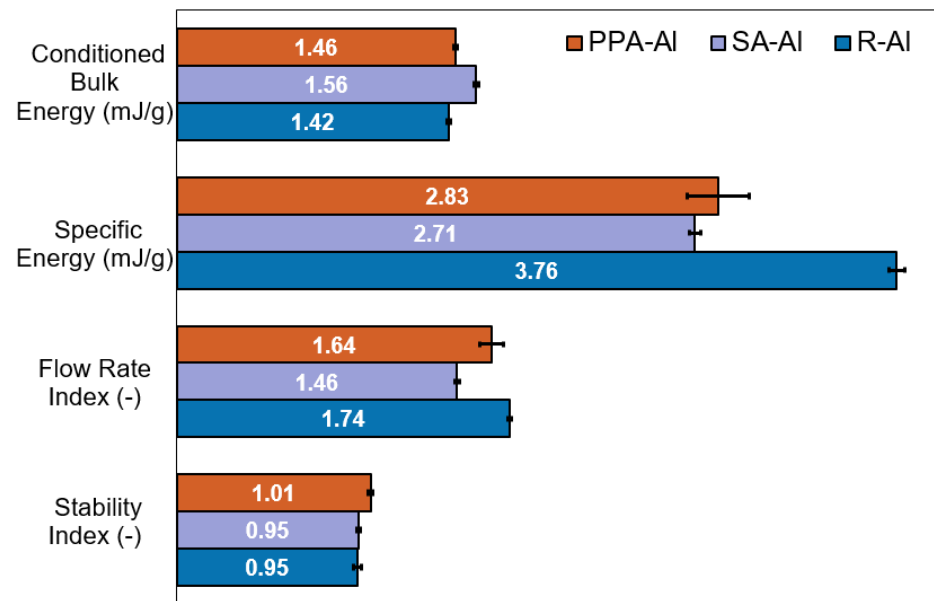


**Figure 6.** Comparison of the values generated using FT4 stability and variable flow rate tests including conditions bulk density, specific energy, flow rate index, and stability index for all raw and treated powders.

Mohr–Coulomb stress circle analysis was used to evaluate the cohesion and flow factor of the raw and surface treated powder samples, as shown in Figure 7. By using four different applied normal stress values, the line can be extrapolated linearly to zero applied normal stress, which gives the cohesion value. Cohesion is a complex property, consisting of many different components, both physical and chemical. The treatment process is intended to remove some of these components, such as interparticulate interactions like capillary bridging due to physisorbed water and direct hydrogen bonding between surface hydroxyls. The method by which the cohesion value is generated is directly related to the measured shear stress with applied normal force. If the surface attractive forces are decreased, the measured shear stress should also decrease. This trend was observed for the surface treated powders when compared to the raw powder control sample. The extrapolated cohesion values for R-AI, SA-AI, and PPA-AI are 0.384, 0.214, and 0.318 kPa, respectively. The SA surface treatment resulted in a 44% reduction in cohesion, while the PA treatment showed a modest decrease by 17%. The flow factor ( $f_c$ ) increased by 33% for the SA-AI sample and PA-AI increased by 20%.

The compressibility of a powder gives an indirect measurement of the cohesion reduction through packing properties. Compressibility curves report the changes in the powder bed height, reported as a percentage, with increasing applied normal stress. Figure 8 reveals the curves for each of the three samples. In both SA-AI and PA-AI, the compressibility percentage was reduced by 42% when compared to the raw material. Powders that have poor packing properties and large interstitial pores have high compressibility due to the release of void air pockets and particle rearrangement with applied normal stress. The RA-AI compressibility data shows a 7% change from 0.5 to 8.0 kPa, whereas SA-AI and PA-AI had a change of about 4%. This finding can be corroborated by the increase in apparent density and reduction in  $H_R$ , as shown previously (Figure 5).

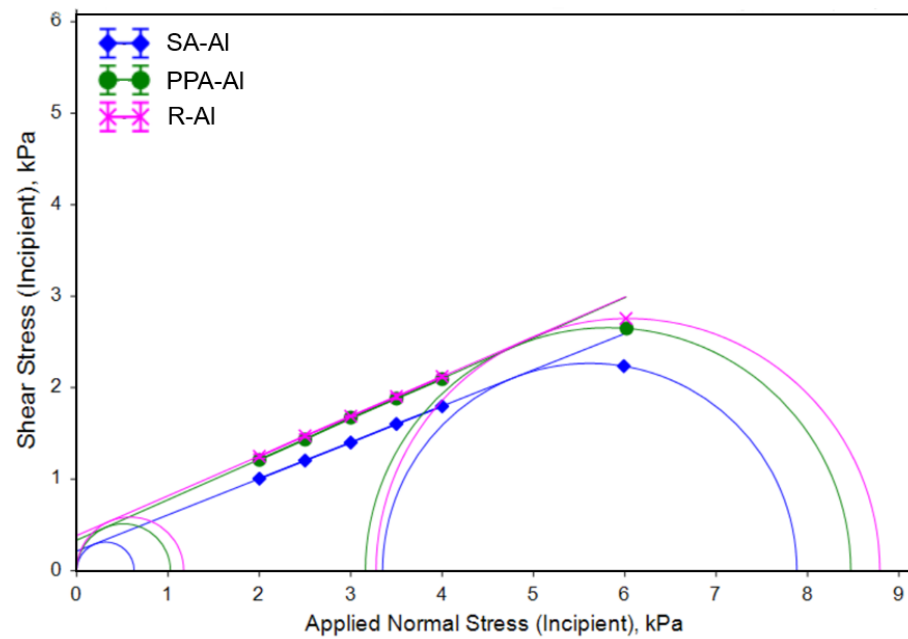


Figure 7. Mohr–Coulomb stress circle analysis of shear data collected for SA-Al, PA-Al, and R-Al.

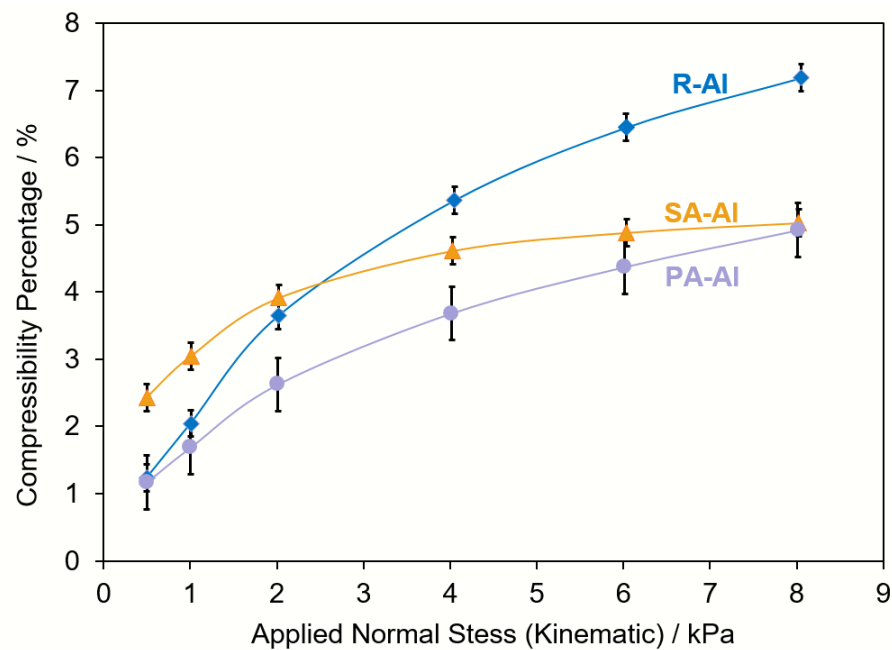


Figure 8. Compressibility curve data for R-Al, SA-Al, PA-Al, showing a compressibility reduction at 8 kPa for SA-Al and PA-Al samples by 42%.

Powder flow is difficult to assess with a single number. For this work, a holistic view of the reference and treated powders was taken through using different types of testing methods, including direct and empirically derived results. Overall, the PPA-Al showed an improvement in flow behavior by using the density-based Hausner Ratio, reduced SE, reduced cohesion, and lowered compressibility. Using the FRI and SI, the PPA-Al powder was not significantly altered in terms of reaction to variable flow rates and multiple conditioning cycles. Similarly, the same trends were observed for the SA-Al. Both surface treatments improved the powders flow properties when compared to the reference material, making them potential candidates for bulk scale surface processing.

#### 4. Conclusions

Metallic aluminum powder has widespread use; however, flow applications can be limited due to the high cohesivity and agglomeration of fine particles. Optimizing its behavior through the use of thin surface coatings further extends its usage into flow based production methods that would typically fail with a poorly flowing material. Finding low-cost, high performance surface coatings is an important area of study for improving powder flow properties. The two coatings are good potential candidates for high performing coatings due to their hydrophobic character when applied to surfaces and relatively low cost for large scale processing.

Both SA and PPA were successfully deposited on aluminum powder particles as shown by DRIFTS and XPS surface analysis. Using DRIFTS, characteristic vibrational modes for each of the treatment molecules were observed when compared to the neat material or literature references. The XPS spectra showed retention of the surface treatment through increased carbon content for SA-Al and the presence of phosphorus in the PPA-Al spectrum.

The flow properties were analyzed using a suite of characterization tools, including density based measurements and powder rheology. The surface treatments resulted in an improvement in flow properties based on the  $H_R$  and the rheologically determined values, including SE, cohesion, and compressibility.

The surface coverage and orientation of the treatment molecules is an important follow on study to this work. While some amount of reagent was retained, there is not a comprehensive understanding of how the molecules were retained. Understanding these properties would allow for optimization of the conditions for a bulk processing method.

**Funding:** This material is based upon work supported by the Office of Naval Research under contract No. N00024-12-D-6402, Delivery Order No. 0037.

**Institutional Review Board Statement:** Not applicable.

**Informed Consent Statement:** Not applicable.

**Data Availability Statement:** Data are contained within the article.

**Acknowledgments:** The author wishes to thank Maria Medeiros for funding this effort.

**Conflicts of Interest:** The author declares no conflict of interest. The funders had no role in the design of the study; in the collection, analyses, or interpretation of data; in the writing of the manuscript, or in the decision to publish the results.

#### Abbreviations

The following abbreviations are used in this manuscript:

$\rho_A$	Apparent density (g/mL)
CBD	Conditioned Bulk Density (g/mL)
DRIFTS	Diffuse Reflectance Infrared Fourier Transform Spectroscopy
FRI	Flow Rate Index (-)
$H_R$	Hausner Ratio (-)
PPA-Al	Phenyl-phosphonic Acid Treated Aluminum Powder
R-Al	Raw aluminum powder
SI	Stability Index (-)
SA	Stearic Acid
SA-Al	Stearic Acid Treated Aluminum Powder
SE	Specific Energy (mJ/g)
$\rho_T$	Tap density (g/mL)
XPS	X-ray photoelectron spectroscopy

## References

1. Palmero, P.; Montanaro, L.; Reveron, H.; Chevalier, J. Surface coating of oxide powders: A new synthesis method to process biomedical grade nano-composites. *Materials* **2014**, *7*, 5012–5037. [[CrossRef](#)]
2. Bidulsky, R.; Gobber, F.; Bidulska, J.; Ceroni, M.; Kvackaj, T.; Marco, A.G. Coated metal powders for laser powder bed fusion (L-PBF) processing: A review. *Metals* **2021**, *11*, 1831. [[CrossRef](#)]
3. Foster, G.; Kempema, N.J.; Boyer, J.E.; Harris, J.R.; Yetter, R.A. Experimental investigation of aluminum-air burning velocity at elevated pressure. *Combust. Flame* **2023**, *248*, 112532. [[CrossRef](#)]
4. Przybyszewski, B.; Boczkowska, A.; Kozera, R.; Mora, J.; Garcia, P.; Aguero, A.; Borrás, A. Hydrophobic and icephobic behaviour of polyurethane-based nanocomposite coatings. *Coatings* **2019**, *9*, 811. [[CrossRef](#)]
5. Jallo, J.; Schoenitz, M.; Dreizin, E.L.; Dave, R.N.; Johnson, C.E. The effect of surface modification of aluminum powder on its flowability, combustion and reactivity. *Powder Technol.* **2010**, *204*, 63–70. [[CrossRef](#)]
6. Chen, Y.; Jallo, J.; Quintanilla, M.A.S.; Dave, R. Characterization of particle and bulk level cohesion reduction of surface modified fine aluminum powders. *Colloids Surf. A* **2010**, *361*, 60–80. [[CrossRef](#)]
7. Ludwig, B.; Miller, T.F. Rheological and surface chemical characterization showing enhanced flowability and fluidization behavior for deliver applications. *Powder Technol.* **2015**, *283*, 380–388. [[CrossRef](#)]
8. Ludwig, B.; Gray, J.L. The effect of gas phase polydimethylsiloxane surface treatment of metallic aluminum particles: Surface characterization and flow behavior. *Particuology* **2017**, *30*, 92–101. [[CrossRef](#)]
9. Johansson, E.; Nyborg, L. XPS study of carboxylic acid layers on oxidized metals with reference to particulate materials. *Surf. Interface Anal.* **2003**, *35*, 375–381. [[CrossRef](#)]
10. Nguyen, D.M.; Vu, T.N.; Nguyen, T.M.L.; Nguyen, T.D.; Thuc, C.N.H.; Bui, Q.B.; Colin, J.; Perré, P. Synergistic influences of stearic acid coating and recycled PET microfibers on the enhanced properties of composite materials. *Materials* **2020**, *13*, 1461. [[CrossRef](#)]
11. Nguyen, T.T.; Nguyen, V.L.; Pham, T.T.H.; Pham, T.T.; Nguyen, T.D. Effects of Surface Modification with Stearic Acid on the Dispersion of Some Inorganic Fillers in PE Matrix. *J. Compos. Sci.* **2021**, *5*, 270. [[CrossRef](#)]
12. Lim, M.S.; Feng, K.; Chen, X.; Wu, N.; Raman, A.; Nightingale, J.; Gawalt, E.S.; Korakakis, D.; Hornak, L.A.; Timperman, A.T. Adsorption and desorption of stearic acid self-assembled monolayers on aluminum oxide. *Langmuir* **2007**, *23*, 2444–2452. [[CrossRef](#)]
13. Zang, D.; Zhu, R.; Zhang, W.; Wu, J.; Yu, X.; Zhang, Y. Stearic acid modified aluminum surfaces with controlled wetting properties and corrosion resistance. *Corros. Sci.* **2014**, *83*, 86–93. [[CrossRef](#)]
14. Li, N.; Zhang, Y.; Guo, R.; Yang, J.; Zhang, X.; Wang, X. Effect of stearic acid coating on the explosion characteristics of aluminum dust. *Fuel* **2022**, *320*, 123880. [[CrossRef](#)]
15. Yagyo, S.; Yoshitake, M.; Tsud, N.; Chikuyow, T. Adsorption structure of phenyl-phosphonic acid on an alumina surface. *Appl. Surf. Sci.* **2009**, *256*, 1140–1143. [[CrossRef](#)]
16. Lee, J.; Bong, J.; Ha, Y.G.; Park, S.; Ju, S. Durability of self-assembled monolayers on aluminum oxide for determining surface wettability. *Appl. Surf. Sci.* **2015**, *330*, 445–448. [[CrossRef](#)]
17. Davies, P.R.; Newton, N.G. The chemisorption of organophosphorous compounds at an Al(111) surface. *Appl. Surf. Sci.* **2001**, *181*, 296–306. [[CrossRef](#)]
18. Aresti, A.; Aragonese, J.; Lopez-Valverde, N.; Suarez, A.; Aragonese, J.M. Effectiveness of Biofunctionalization of Titanium Surfaces with Phosphonic Acid. *Biomedicines* **2021**, *9*, 1663. [[CrossRef](#)]
19. Zhao, R.; Rupper, P.; Gaan, S. Recent Development in Phosphonic Acid-Based Organic Coatings on Aluminum. *Coatings* **2017**, *7*, 133–154. [[CrossRef](#)]
20. Thissen, P.; Valtiner, M.; Grundmeier, G. Stability of phosphonic acid self-assembled monolayers on amorphous and single crystal aluminum oxide surfaces in aqueous solution. *Langmuir* **2010**, *26*, 156–164. [[CrossRef](#)]
21. ASTM, B527-06; Standard Test Method for Determination of Tap Density of Metallic Powders and Compounds. ASTM International: West Conshohocken, PA, USA, 2006.
22. Hausner, H.H. Friction conditions in a mass of metal powder. *J. Powder Metall.* **1967**, *3*, 7–13.
23. Dote, J.L.; Mowery, R.L. Infrared reflectance-absorption spectra of Langmuir-Blodgett stearic acid monolayers on gold and aluminum, influence of substrate. *J. Phys. Chem.* **1988**, *92*, 1571–1575. [[CrossRef](#)]
24. Morterra, C.; Magnacca, G. A case study: Surface chemistry and surface structure of catalytic alumina as studied by vibrational spectroscopy of adsorbed species. *J. Catal. Today* **1996**, *27*, 497. [[CrossRef](#)]
25. Silverstein, R.M.; Webster, F.X. *Spectrometric Identification of Organic Compounds*, 6th ed.; Wiley: Hoboken, NJ, USA 1998; p. 142.
26. Raman, A.; Quinones, R.; Barriger, L.; Eastman, R.; Parsi, A.; Gawalt, E.S. Understanding Organic Film Behavior on Alloy and Metal Oxides. *Langmuir* **2009**, *26*, 1747–1754. [[CrossRef](#)]
27. Koh, S.E.; McDonald, K.D.; Holt, D.H.; Dulcey, C.S.; Chaney, J.A.; Pehrsson, P.E. Phenylphosphonic Acid Functionalization of Indium Tin Oxide: Surface Chemistry and Work Functions. *Langmuir* **2006**, *22*, 6249–6255. [[CrossRef](#)]

**Disclaimer/Publisher’s Note:** The statements, opinions and data contained in all publications are solely those of the individual author(s) and contributor(s) and not of MDPI and/or the editor(s). MDPI and/or the editor(s) disclaim responsibility for any injury to people or property resulting from any ideas, methods, instructions or products referred to in the content.